Impact of the Pedestal on Global Performance and Confinement Scalings in I-Mode

J. R. Walk[1], J. W. Hughes[1], A. E. Hubbard[1], D. G. Whyte[1], A. E. White[1]

[1] MIT Plasma Science and Fusion Center, 77 Massachusetts Avenue, Cambridge, MA 02139

E-mail: jrwalk@psfc.mit.edu

Abstract. I-mode is a novel alternate high-confinement tokamak regime, notable for the formation of a strong temperature pedestal with associated H-mode-like increase in energy confinement, without the accompanying density pedestal or suppression of particle transport. I-mode exhibits a number of attractive features for a tokamak reactor regime, namely (1) an inherent lack of large, deleterious Edge-Localized Modes (ELMs), (2) minimal impurity accumulation and radiative loss compared to conventional H-modes, and (3) an apparent lack of strong degradation of energy confinement with input heating power. Previous analyses of I-mode experiments at Alcator C-Mod have elucidated the pedestal structure in I-mode, particularly in its strong positive response to fueling and input heating power. Global performance and confinement responds accordingly to these inputs, with both absolute (*e.g.,* plasma stored energy) and normalized (*e.g.,* β_N) metrics responding strongly to fueling and heating power. Due to core temperature profile stiffness, the very high pedestal temperature in I-mode results in comparable core and global-averaged pressures to H-mode despite the relaxed density profile, although moderate levels of density peaking are still observed. The minimal degradation of energy confinement time with heating power in I-mode is also observed empirically, in contrast to the strong ($\tau_E \sim P^{-0.7}$) degradation found in H-mode. Following the practices of the multi-machine ITER89 and ITER98 confinement scalings for L-mode and ELMy H-mode respectively, an initial assay at a confinement scaling for I-mode is also presented. The single-machine scaling captures the observed physics in I-mode, and extrapolates highly favorably to large, high-field, high-power devices, motivating further I-mode experiments on larger tokamak experiments.

PACS numbers: 52.55.Fa,52.55.Tn,52.25.Fi,52.40.Hf,52.35.Py

1. Introduction

Viable & economical power generation via tokamak magnetic-confinement fusion is characterized by two seemingly-contradictory requirements. First, a high level of energy confinement is necessary for the desired level of self-heating by fusion products (*e.g.,* "alpha heating" for deuterium-tritium fusion) for net energy production. At the same time, particle confinement must be sufficiently low to avoid the deleterious effects of accumulated impurities (both the helium "fusion ash" and high-Z materials introduced from eroded plasma-facing surfaces) due to fuel dilution and radiative losses. The energy confinement requirement has been achieved in a class of operating regimes, collectively termed "H-modes" [1], characterized by the formation of an edge transport barrier, termed the *pedestal*, characterized by steep gradients in density, temperature, and pressure, with H-modes capable of stationary operation requiring a relaxation mechanism on the density pedestal to avoid impurity accumulation.

While the height of the pedestal is strongly correlated with global fusion performance [2], the strong gradients inherent in the pedestal have been shown to drive edge MHD instabilities [3, 4, 5] resulting in an Edge-Localized Mode (ELM), an explosive perturbation to the pedestal driving a rapid burst of energy and particle transport into the plasma exhaust [6]. On existing devices, these bursts of transport are sufficient to vent accumulated impurities from the plasma, allowing stationary operation with acceptable radiative losses [7]. As the ELMy H-mode is robust and relatively straightforward to achieve, the regime is considered the baseline for high-confinement operation on ITER [8, 9]. However, on ITER- or reactor-scale devices ELMs drive transient heat loads to the divertor, leading to unacceptable levels of erosion and heat damage to plasma-facing components [10, 11]. As such, the avoidance, suppression, or mitigation of large ELMs, either via externally-applied engineering solutions (pellet pacing [12, 13] or resonant magnetic perturbations [14, 15]), or via alternate high-confinement regimes which regulate the pedestal below the ELM stability limit (*e.g.,* the Enhance D_α (EDA) H-mode [16, 17] or QH-mode [18, 19]).

The I-mode [20, 21, 22, 23], pioneered on the Alcator C-Mod tokamak [24], is a promising new regime for high-performance operation. I-mode is unique among high-performance regimes in that it evidently decouples energy and particle transport – the regime develops a strong temperature pedestal and associated H-mode-like energy confinement improvement, while retaining an L-mode-like density profile lacking a pedestal or suppression of particle transport as in conventional H-modes (see Figure 1). I-mode operation offers several attractive features for a reactor regime: (1) relaxed density profile providing desirable L-mode-like levels of impurity accumulation [25], (2) an inherent lack of large ELMs, avoiding the need for externally-applied ELM control, and (3) minimal degradation of energy confinement with heating power [20, 26], in contrast to the degradation found in ELMy H-mode (roughly $\tau_E \sim P^{-0.7}$ [8, 27]).

Good progress has been made in understanding the pedestal structure and stability in I-mode [22, 23], particularly regarding the pedestal response to engineering inputs and

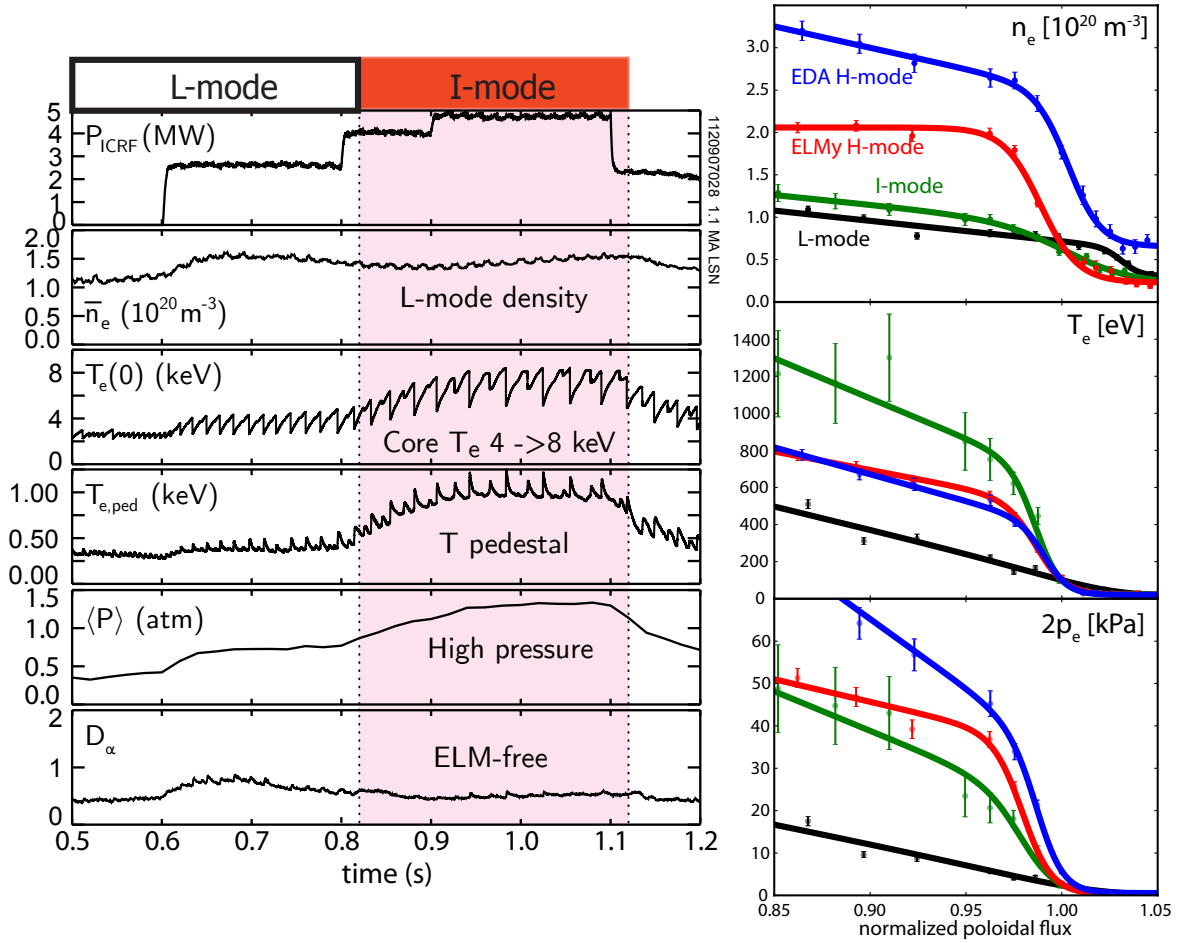

Figure 1: (left) characteristic time traces for an I-mode. After the L-I transition, the core and edge temperature rise over several sawtooth cycles (visible in the oscillations in $T_e(0)$ and $T_{e,ped}$) before reaching a steady level; global pressure and confinement rise accordingly. However, the density remains unchanged from the L-mode level. No ELMs are exhibited on the D_α trace. (right) pedestal profiles for L-, I-, and H-modes. The I-mode (green) retains a density profile similar to L-mode (black), unlike the ELMy (red) and EDA (blue) H-modes, which form a strong density pedestal. However, the I-mode forms a higher temperature pedestal than either H-mode, resulting in comparable pedestal pressures to H-mode while retaining L-mode particle transport.

stability against the MHD triggers associated with the ELM. However, the development of I-mode as a viable reactor regime requires further understanding of the access and extrapolation of the mode to larger tokamak experiments, and its potential for desirable levels of performance on those devices. In this paper, we first review the the responses of pedestal and core profiles (Section 2), and their impact on normalized performance (*e.g.*, volume-averaged β_N) and confinement. Second, following the practices of the ITER89 [27, 28] and ITER98 [8] exercises, we establish an initial assay into a new confinement scaling for I-mode (Section 3) encompassing C-Mod data, with connections to empirical

observation. Lastly, we examine possible size dependences for the energy confinement, and subsequent extrapolations to larger devices (Section 4).

add intro section on I-mode access?

2. Profiles and Responses

2.1. Pedestal Profiles

A firm understanding of the pedestal is necessary for the establishment of the I-mode as a viable reactor regime. To this end, a series of dedicated experiments [22, 23] was conducted to examine the pedestal structure and stability in I-mode. A scan of plasma current from 0.85 to 1.35 MA in a reversed-field, lower-null shape reveals a strong positive trend of pedestal electron temperature with current (Fig. 2) with the I-mode pedestal T_e (for this paper, we use the pedestal parameters evaluated at the 95% flux surface) meeting or exceeding H-mode levels at comparable plasma current.

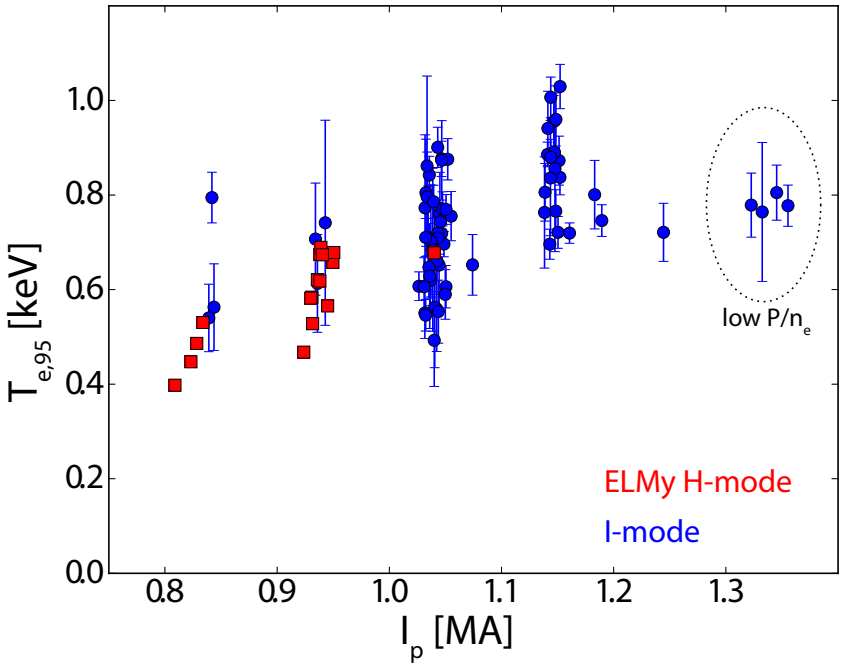

Figure 2: Pedestal temperature versus plasma current, comparing ELMy H-modes and I-modes. Notably, I-mode pedestal temperatures meet or exceed H-mode levels at comparable temperature, and trend positively with plasma current. The spread at fixed current is due to varying power per particle (see Fig. 3)

However, there is significant spread at fixed I_p, due to the wide variation in input heating power. Examining a single current slice (Fig. 3) at 1.15 MA, we see a strong dependence of the pedestal temperature on net heating power, $P_{net} = P_{ICRF} + P_{Ohm} - P_{rad} - dW/dt$, normalized to the density (effectively, input heating power per particle).

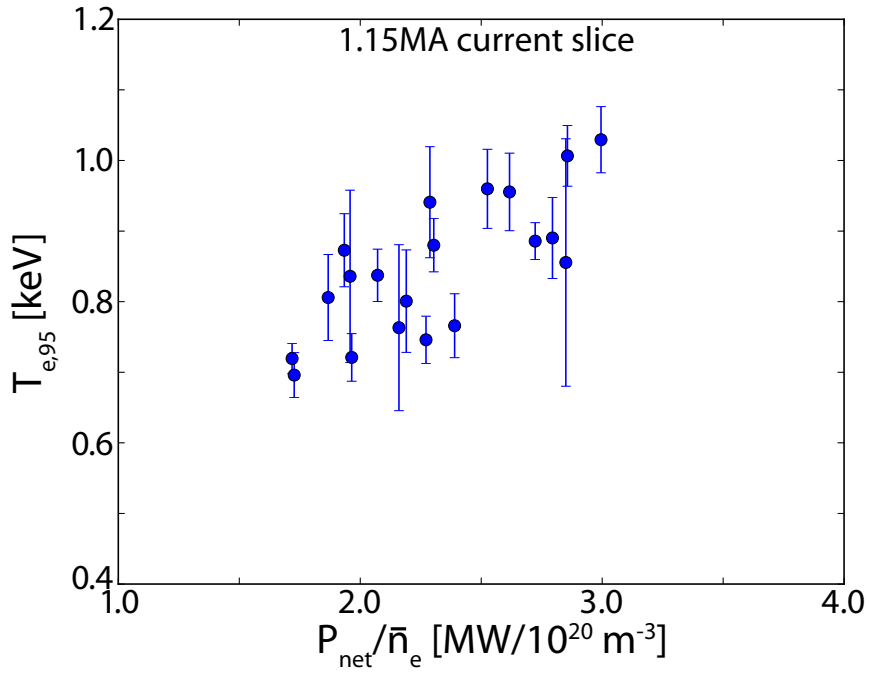

Figure 3: Pedestal temperature versus heating power normalized to average density – effectively, power per particle – at $I_p = 1.15$ MA, illustrating an approximate linear trend of the pedestal T_e with $P_{net}/\overline{n}_e$ ($P_{net} = P_{ICRF} + P_{Ohm} - P_{rad} - dW/dt$)

In contrast to the temperature pedestal, the L-mode-like density profile in I-mode is set primarily through operator fueling via gas puffing. Given sufficient heating power, temperature pedestals can be maintained alongside increased fueling across a broad range. Example discharges matched in current, field, and shaping are shown in Fig. 4, spanning a range in fueling and heating power, $\overline{n}_e = 1.0 - 1.7 \times 10^{20}$ m^{-3}, $P_{net} = 2.75 - 4.10$ MW. Temperature pedestals are matched across all three discharges despite the variation in fueling levels and edge densities, using consistent power per particle, $P_{net}/\overline{n}_e = 2.4 - 2.7$ MW/10^{20}m^{-3}.

This behavior is distinct from that found in H-modes on C-Mod – ELMy H-modes are limited, to good approximation, at a fixed pedestal β_p determined by shaping, driving an inverse relationship between pedestal n_e and T_e at a given current, while transport-limited EDA H-modes lack operator control of the pedestal density at a given plasma current. Independent control of the pedestal density and temperature profiles allows optimization of the energy confinement, fueling, and impurity venting for improved performance. The pedestal β_p and global performance may be strongly improved via matched increases in fueling and heating power (maintaining the target $P_{net}/\overline{n}_e$ for the temperature pedestal) after accessing the regime at lower power and density access for ITER?

add pedestal pressure vs Wmhd?

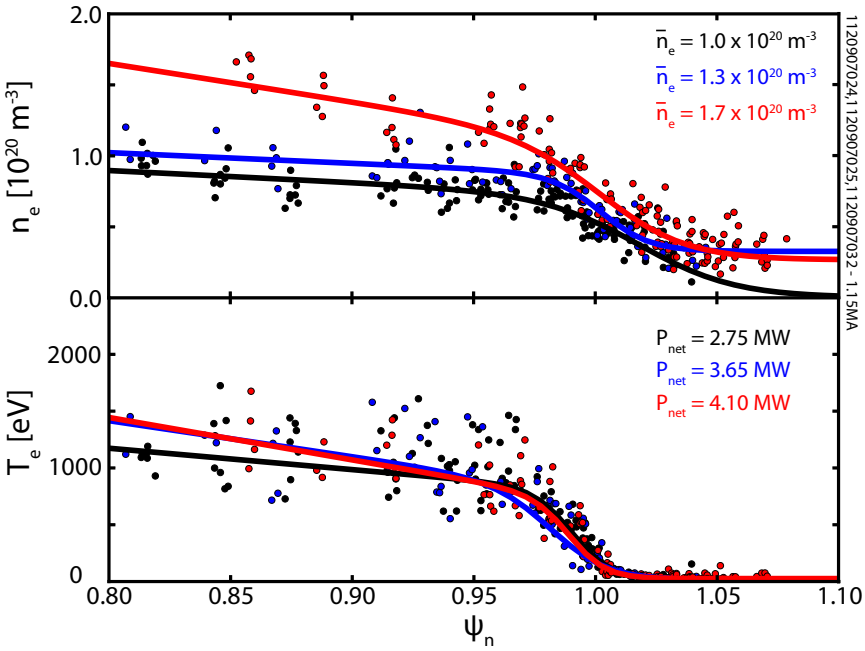

Figure 4: Three discharges, matched in current (1.1 MA), field (5.6 T), and shaping, fueled to $\overline{n}_e = 1.0, 1.3, 1.7{\times}10^{20}$ m^{-3}, spanning a large fraction of the density range in the I-mode discharges presented here. With sufficient heating power (2.75, 3.65, 4.10 MW), temperature pedestals can be matched across the fueling range. This corresponds to power-per-particle values of $P_{net}/\overline{n}_e \sim 2.4 - 2.7$ MW/10^{20}m^{-3}.

2.2. Core Profiles

The high pedestal temperature in I-mode, coupled with core profile stiffness (such that higher temperatures supports a steeper marginally-stable ∇T_e), supports very high core temperatures add I-mode T_e stiffness. With a moderate degree of core density peaking (with typical values of $n_{e0}/\langle n_e \rangle \sim 1.1{-}1.3$, comparable to H-mode) add density peaking, this supports comparable core and volume-averaged pressures to H-mode despite the comparatively relaxed pressure pedestal, supporting beneficial fusion conditions in the core while avoiding stability issues in the pedestal. Example density, temperature, and pressure profiles for I-mode and H-mode are shown in Fig. 5, illustrating the high core pressure attainable in I-mode despite the relaxed pedestal and lower density.

Accordingly, I-modes on C-Mod inhabit a comparable range in global confinement metrics, as shown in Fig. 6. In both global normalized beta ($\langle \beta_N \rangle = \langle \beta \rangle a B_T / I_p$) and normalized confinement H_{98}, the I-mode occupies a comparable range to ELMy H-mode, indicating competitive levels of global confinement while maintaining desirable ELM stability and impurity confinement behaviors.

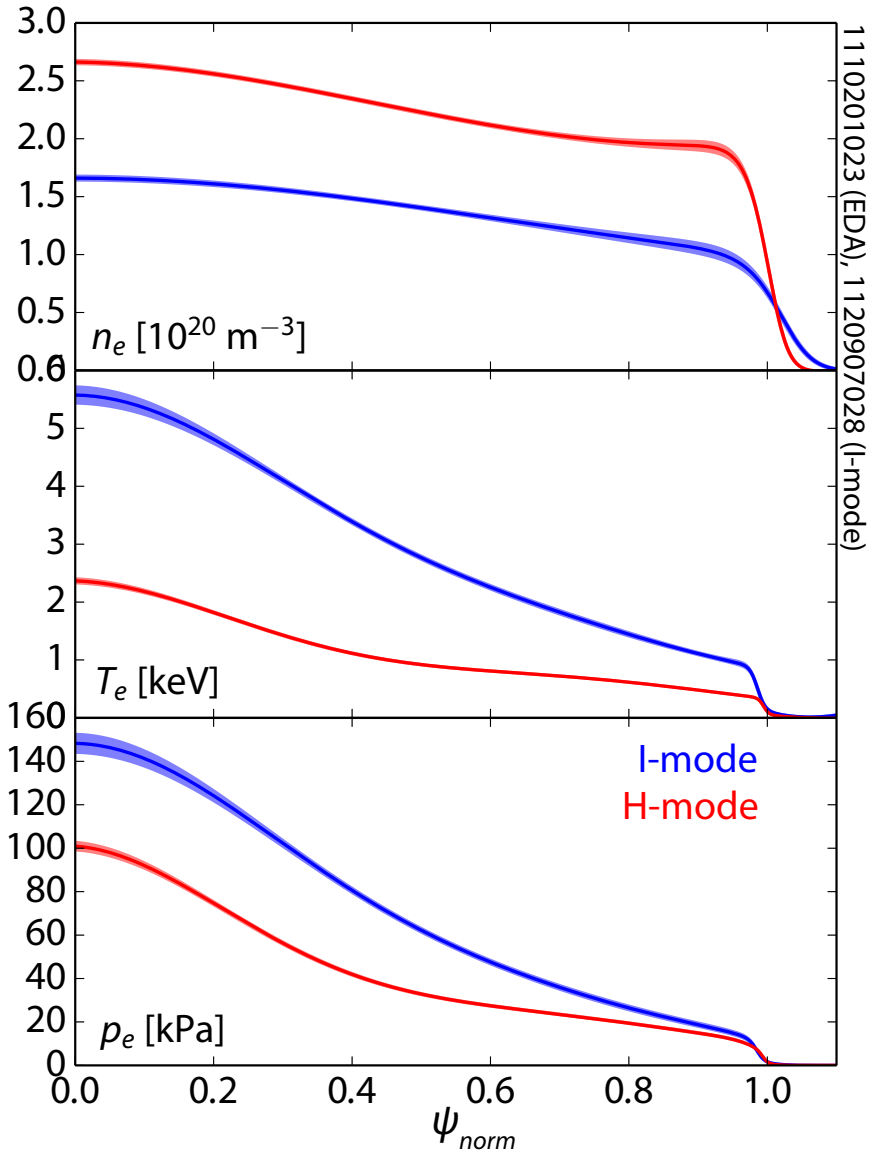

Figure 5: Profiles in electron density, temperature, and pressure for I-mode and EDA H-mode, with $\pm\sigma$ errorbars indicated by the shaded region. The H-mode case exhibits a very strong density pedestal, with a somewhat reduced temperature pedestal; the I-mode, in contrast, has a significant temperature pedestal with a relaxed density profile. While this typically results in a reduced pedestal pressure in I-mode compared to H-mode, core profile stiffness supports very high central temperatures, such that I-mode exhibits comparable or greater core and average pressure despite the relaxed pedestal.

3. I-Mode Confinement Scalings

Due to the complexities inherent in the processes responsible for energy trasport – both short-wavelength drift-wave turbulence and longer-wavelength MHD processes – it is difficult to model energy confinement from first principles. Rather, it is common to

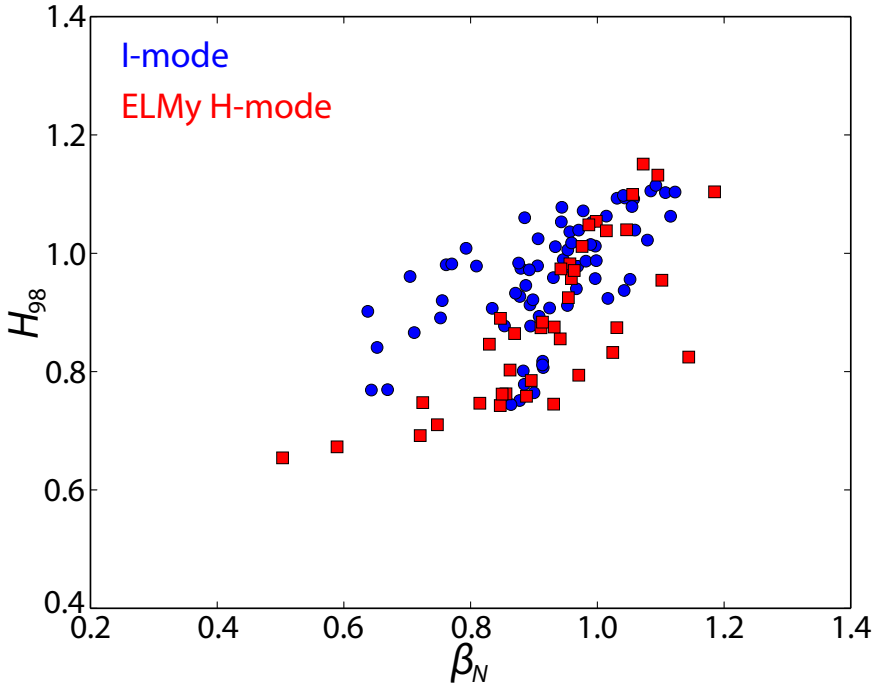

Figure 6: Global normalizezd β_N versus confinement factor H_{98} for I-mode and ELMy H-mode. Despite the relaxed pedestal pressure, I-modes reach comparable average pressures, while maintaining H-mode-like energy confinement.

establish empirical scaling laws for energy confinement using a power-law fit to large datasets. For example, the ITER89 [28] and ITER98 [8] exercises utilized an extensive multi-machine database [27] for L-mode and ELMy H-mode confinement respectively. In particular, the ITER98y2 scaling is used as a common baseline for performance in high-confinement regimes, particularly in terms of its normalized factor H_{98} define this? earlier?

While the H_{98} factor is commonly used as a figure of merit for high-performance regimes (particularly, ELM-suppressed H-modes developed more recently than the ITER98 scaling exercise), it is, effectively, simply a measurement of the quality of the ITER98 prediction to the data. As the ITER98 scaling was constructed using predominantly ELMy H-modes, it implicitly includes the physics of ELM-limited pedestals – for confinement regimes governed by substantially different physics, this is not necessarily a good prediction. While I-mode data is currently largely limited to C-Mod, and is insufficient for a full confinement scaling (particularly, to develop the dependence on machine size), it is nonetheless illustrative to examine a dedicated I-mode confinement scaling.

I-mode energy confinement times are fitted in an ordinary least-squares sense to an ITER98-like power law of the form

$$\tau_{I-mode} = C\ I_p^{\alpha_{I_p}}\ B_T^{\alpha_{B_T}}\ \overline{n}_e^{\alpha_{n_e}}\ R^{\alpha_R}\ \varepsilon^{\alpha_\varepsilon}\ \kappa^{\alpha_\kappa}\ P_{loss}^{\alpha_P} \tag{1}$$

to find free exponents α_j for plasma current I_p in MA, toroidal field B_T in T, line-

averaged density $\overline{n}_e$ in 10^{20} m^{-3}, major radius R in m, inverse aspect ratio ε, elongation κ, and loss power $P_{loss} = P_{Ohm} + P_{ICRF} - dW/dt$ in MW. Although the net power P_{net} has been demonstrated to be the more suitable parameter, rather than P_{loss} [29], we use P_{loss} here for consistency with previous scaling exercises, and to enable the use of older I-mode data without consistent measurements of the radiated power. However, the radiated power is typically a small fraction of the total power in I-mode ($P_{rad} < 900$ kW, $P_{rad}/P_{tot} < 20\%$), so this is sufficient for an initial assessment of the confinement.

Results from the fitting exercise are shown in Table 1, containing the values and standard deviations for each exponent, the scale factor C, and the r^2 coefficient of determination for the fit. Fit (a) in the table uses the full parameter list used in the ITER98y2 scaling figure?. However, it is immediately obvious that the size scalings, dependent on major radius R and aspect ratio ε, are not properly captured (denoted by the extreme errorbars on these exponents). This is to be expected – absent meaningful variation in R and ε in the dataset (which requires multiple machines to produce) these parameters are not well-constrained, and result (a) is over-fitted. These parameters are omitted in result (b), yielding a minimum-complexity fit on I_p, B_T, $\overline{n}_e$, and P_{loss}. The results of this fit are shown in Figure 7, with the data distinguished between older reversed-field LSN and forward-field USN discharges, as well as a newer dedicated pedestal profile database [22].

α_j	(a)	(b)
C	0.040 ± 0.066	0.014 ± 0.002
I_p	0.686 ± 0.074	0.685 ± 0.076
B_T	0.698 ± 0.075	0.768 ± 0.072
$\overline{n}_e$	-0.077 ± 0.055	0.017 ± 0.048
R	4.219 ± 4.623	
ε	0.127 ± 1.144	
κ	1.686 ± 0.398	
P_{loss}	-0.197 ± 0.048	-0.286 ± 0.042
r^2	0.713	0.685

Table 1: Parameters for the power-law scalings for I-mode energy confinement time τ_E, along with r^2 coefficients of determination for the fit. The full ITER98-like fit (a) is over-constrained, lacking sufficient range in the data to fit R, ε, and κ. These parameters are omitted in the minimum-complexity fit (b). Parameters are in the given units: I_p in MA, B_T in T, $\overline{n}_e$ in 10^{20} m^{-3}, R in m, and P_{loss} in MW. Elongation κ and inverse aspect ratio ε are dimensionless.

A comparison of the results from the minimum-complexity I-mode fit

$$\tau_{I-mode} = 0.014 \times I_p^{0.685}\ B_T^{0.768}\ \overline{n}_e^{0.017}\ P_{loss}^{-0.286} \tag{2}$$

against the corresponding parameters from the ITER89 and ITER98y2 scalings is shown in Table 2. Notably, the I-mode fit exhibits a much stronger dependence on

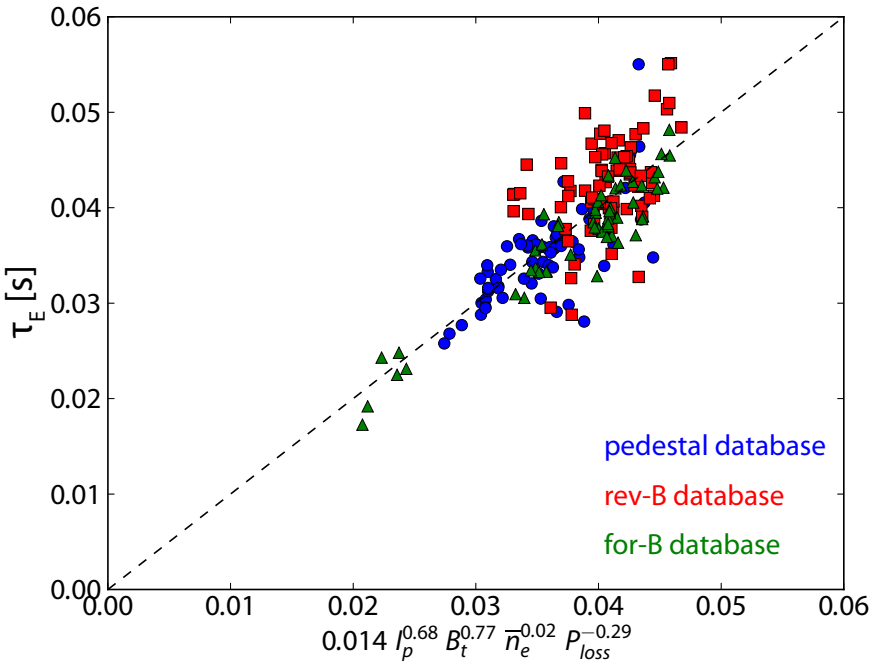

Figure 7: C-Mod I-mode data from older reversed-field and forward-field databases, as well as the newer dedicated pedestal database, showing measured energy confinement time τ_E versus the minimum-complexity fit from Table 1. R^2 coefficient of determination for the fit is 0.685.

magnetic field, and weaker degradation of the confinement with heating power, compared to either the L-mode or H-mode fits. This is consistent with the observed behavior in I-mode, both on C-Mod and elsewhere. The threshold power for the transition to H-mode (which brackets the upper range of the I-mode operational window) typically is strongly elevated with increasing magnetic field [30]; however, the L-I threshold does not meaningfully vary with magnetic field. Thus, the increased magnetic field broadens the operational window for I-mode, as shown in Figure 8. The strong dependence of the confinement on B_T may be explained by the more aggressive pedestals possible at higher field while avoiding the H-mode transition. Similarly, the weak power degradation in the I-mode τ_E is reflected in experimental observations of the plasma stored energy in relation to the plasma current and heating power (Figure 9).

3.1. Normalized Confinement

We may define a normalized confinement factor for the I-mode confinement, analogous to the H_{98} confinement factor, using the fitted τ_{I-mode} from Equation 2:

$$H_{I-mode} = \frac{\tau_E}{\tau_{I-mode}} \tag{3}$$

Trends in H_{I-mode} and H_{98} for I-mode data are shown in Figures 10 and 11. The I-mode scaling preserves the positive trend of normalized confinement with global β_N

α_j	ITER89	ITER98y2	I-mode	
I_p	0.85	0.93	0.69	
B_T	0.2	0.15	0.77	much stronger field dependence
$\overline{n}_e$	0.1	0.41	0.02	
P_{loss}	-0.5	-0.69	-0.29	weak power degradation
R	1.5	2		need other machine input
ε	0.3	0.5		
κ	0.5	0.78		

Table 2: Comparison of power-law exponents for the ITER89 and ITER98y2 fits, and the minimum-complexity I-mode fit. In particular, the I-mode fit exhibits a much stronger dependence on toroidal field, and weaker degradation with input heating power.

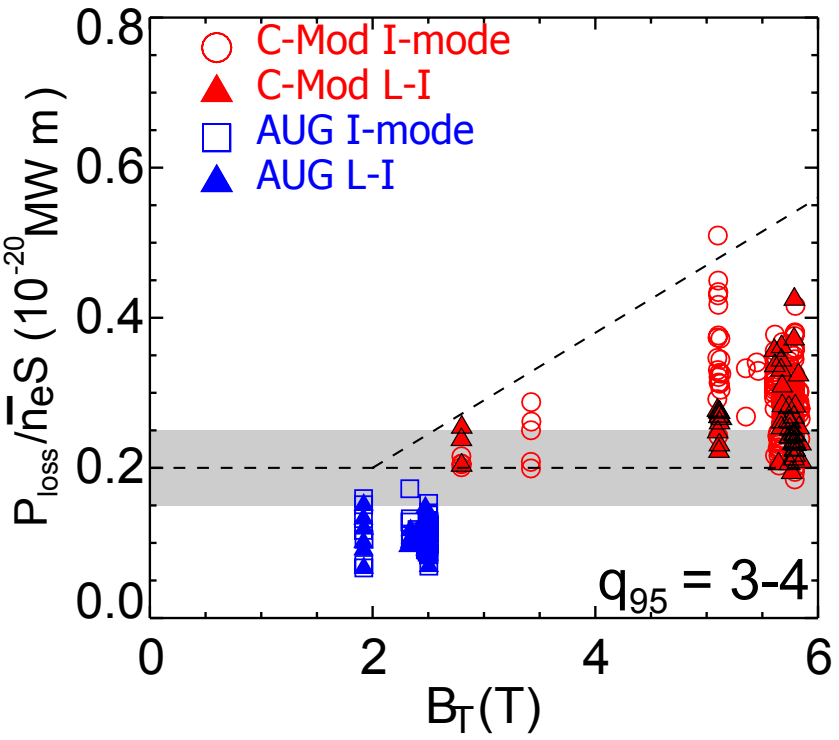

Figure 8: work out caption with Amanda?

found in H-mode (effectively, this is simply the vertical spread in the data cluster seen in Figure 7). I-mode data do not appear to exhibit systematic degradation of (normalized) confinement with increased density – however, this is likely due to the typically lower Greenwald fraction ($< 40\%$) in I-mode. However, the highest normalized confinement cases do occur at the lower end of the density range, largely due to the lower radiated-power fraction and improved $P_{net}/\overline{n}_e$ in these cases (the highest currents and densities were limited in P_{net} by the available power ceiling on C-Mod).

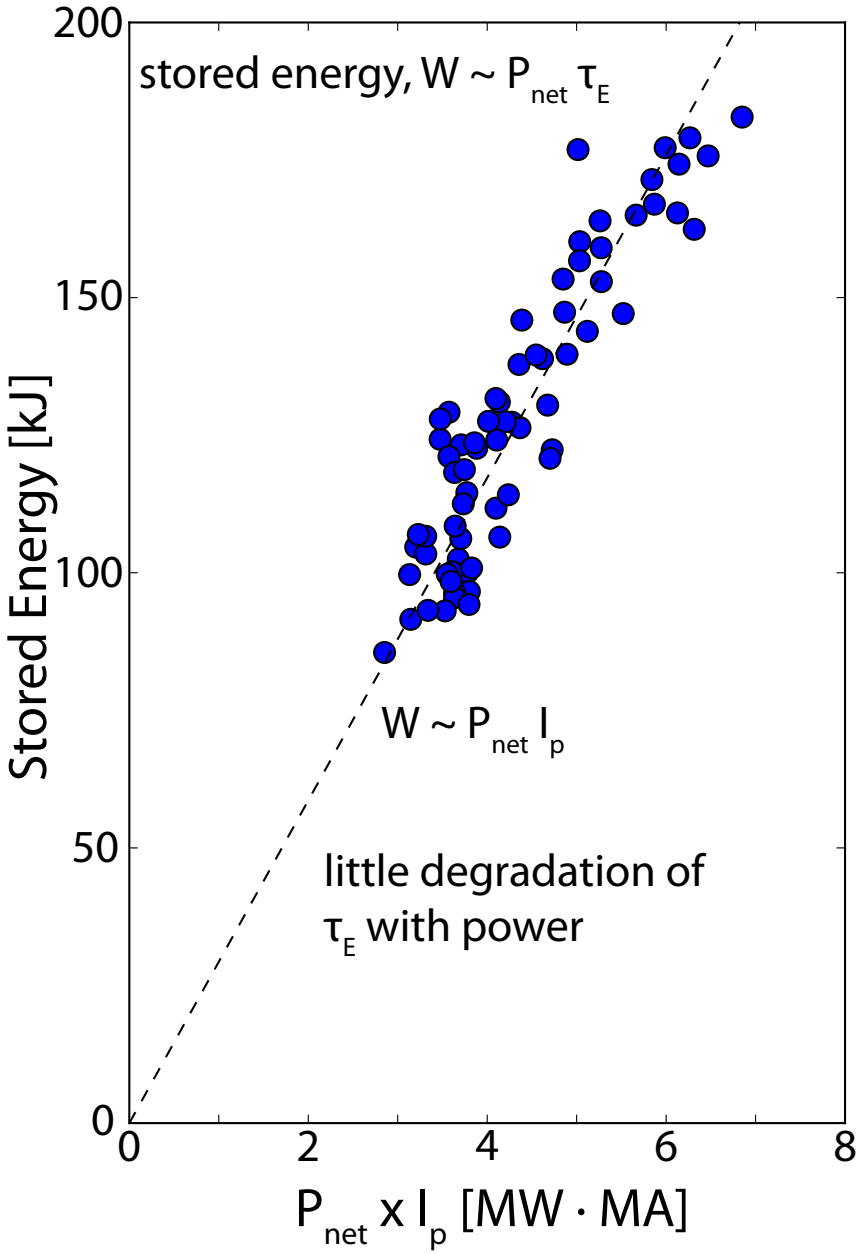

Figure 9: I-mode stored energy versus the product of net heating power P_{net} and plasma current I_p. Based on the H-mode confinement scaling, τ_E is expected to scale linearly with I_p, and to show a strong degradation with heating power, $\tau_E \sim I_p \times P^{-0.7}$. As the stored energy is given by $W \sim P\tau_E$, this should yield $W \sim I_p P_{net}^{0.3}$. The observed linear trend is consistent with little degradation of τ_E in I-mode with heating power. exchange for fixed-current version?

3.2. Covariances

Naturally, in such a scaling exercise covariances between parameters used in the fit are of some concern – hidden dependences between ostensibly-free variables can skew the

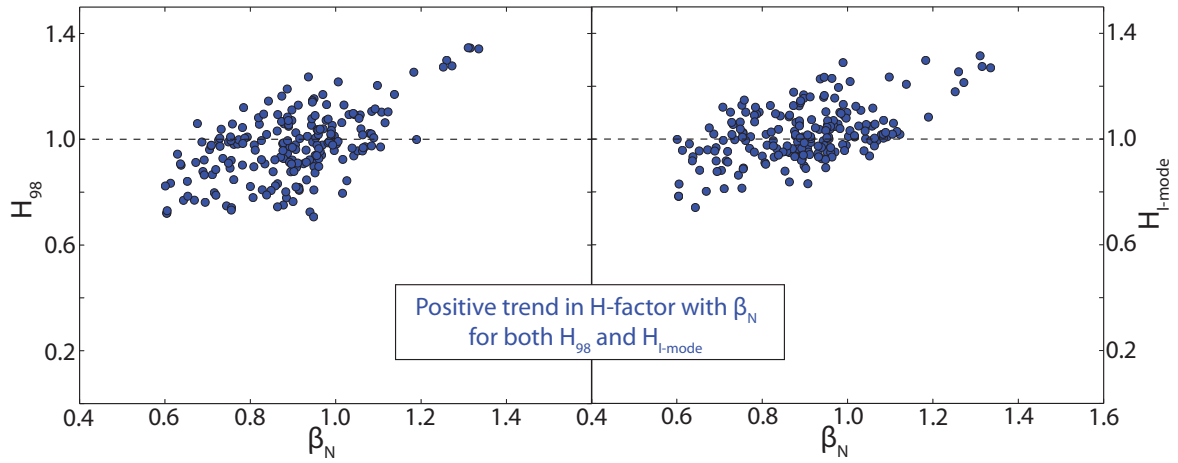

Figure 10: Confinement normalized to the ITER98y2 (left) and I-mode (right) scalings, versus volume-average β_N. In both, a positive trend of normalized confinement with beta is observed, consistent with observations in H-mode.

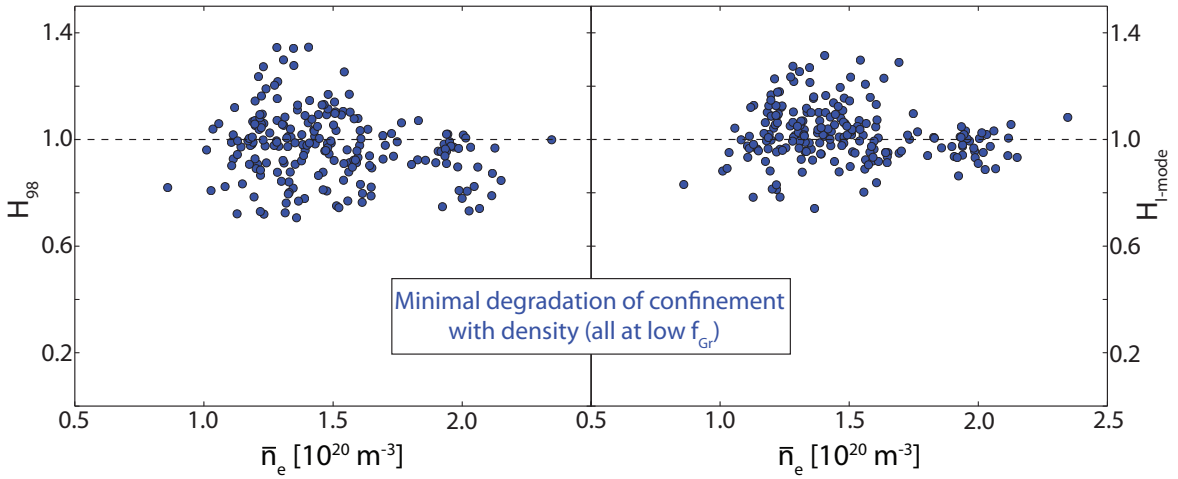

Figure 11: Confinement normalized to the ITER98y2 (left) and I-mode (right) scalings, versus line-averaged density $\overline{n}_e$. Neither case shows significant degradation of confinement with density (unlike H-mode) although the highest normalized-confinement cases do occur at lower density (largely due to the lower radiated-power fraction in these cases).

results of the power-law fit. In the ITER89 and ITER98 scaling exercises, this was addressed in part simply by using as extensive a dataset as possible, ensuring sufficient coverage of a broad range in the chosen parameters. For the more limited dataset of C-Mod I-modes used in this exercise, care must be taken to address possible strong covariances in the data parameters.

Covariance between plasma current I_p and line-averaged density $\overline{n}_e$ (Figure 12) is to be expected, as the gas-puff fueling system operates with a target density within a range

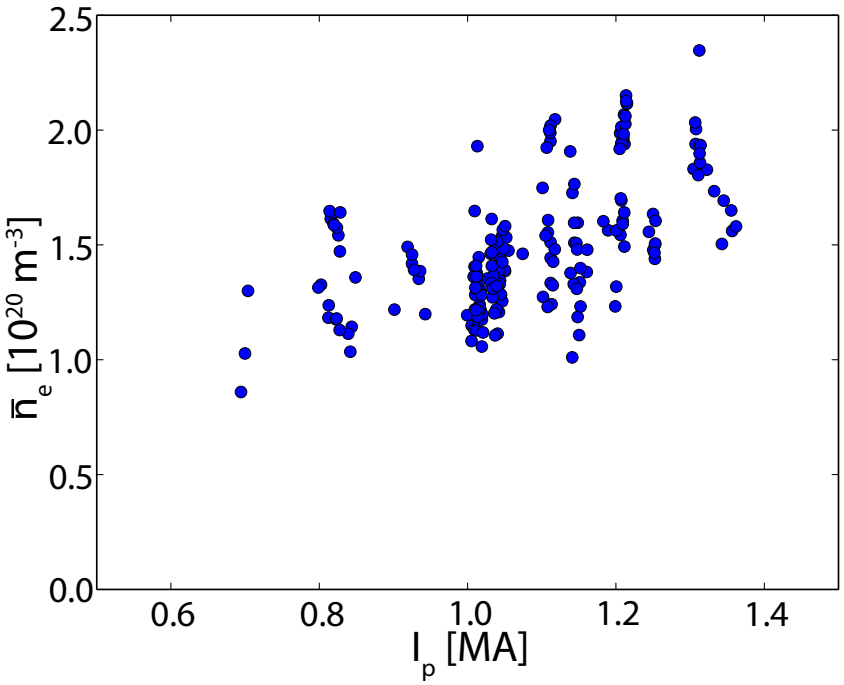

Figure 12: Plasma current I_p versus line-averaged density $\overline{n}_e$ in the I-mode dataset. Though there is a general increasing trend of the density with plasma current, the density is sufficiently freely set by fueling (with Greenwald fraction varying between 0.15 and 0.40) to avoid strong covariance between I_p and $\overline{n}_e$.

determined by the Greenwald density limit ($n_{Gr} = I_p/(\pi a^2)$) cite. However, within this range the target density in I-mode is generally freely variable, albeit at typically lower Greenwald fractions ($f_{Gr} \sim 0.15 - 0.40$) – this is distinct from, for example, transport-limited EDA H-modes on C-Mod, which typically lock to a fixed density set by the plasma current once the H-mode is established cite. As such, while there is a generally-increasing trend of the density with plasma current, the data at any given current point span $> 50\%$ of the total density range, with acceptably low covariance between the parameters.

The interplay between toroidal field B_T and plasma current I_p (Figure 13) is determined by requirements on the edge safety factor $q_{95} \sim B_T/I_p$. As such, there is a distinct positive trend in the *minimum* B_T at a given current with I_p, set by the requirements of minimum q_{95} ($q_{95} > 2.7$ in this dataset) set by global kink limits. However, above this lower bound I-mode access is largely insensitive to the edge safety factor access section? include figure?, allowing the toroidal field to span up to the maximum of the dataset (~ 6 T) across the current range.

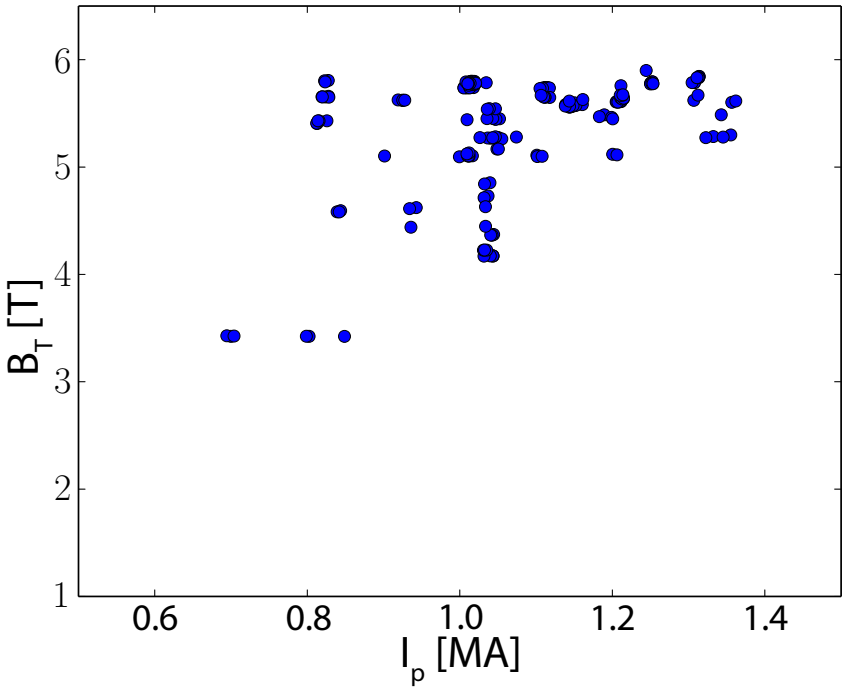

Figure 13: Plasma current I_p versus toroidal field B_T in the I-mode dataset. A positive trend occurs in the *minimum* B_T at a given current, due to the necessity of minimum edge safety factor. Beyond that limit, however, I-mode access is tolerant of a range of edge safety factors, with the $2.7 < q_{95} < 5.3$ (with most of the dataset concentrated in $3 < q_{95} < 4$)

4. Extrapolation to Larger Devices

5. Conclusions

References

[1] F. Wagner, G. Becker, K. Behringer, D. Campbell, A. Eberhagen, W. Engelhardt, G. Fussmann, O. Gehre, J. Gernhardt, G. v. Gierke, G. Haas, M. Huang, F. Karger, M. Keilhacker, O. Klüber, M. Kornherr, K. Lackner, G. Lisitano, G. G. Lister, H. M. Mayer, D. Meisel, E. R. Müller, H. Murmann, H. Niedermeyer, W. Poschenrieder, H. Rapp, H. Röhr, F. Schneider, G. Siller, E. Speth, A. Stäbler, K. H. Steuer, G. Venus, O. Vollmer, and Z. Yü. Regime of improved confinement and high beta in neutral-beam-heated divertor discharges of the ASDEX tokamak. *Physical Review Letters*, 49(19):1408–1412, Nov 1982.

[2] J. E. Kinsey, G. M. Staebler, J. Candy, R. E. Waltz, and R. V. Budny. ITER predictions using the GYRO verified and experimentally validated trapped gyro-Landau fluid transport model. *Nuclear Fusion*, 51(8):083001, 2011.

[3] G. T. A. Huysmans. ELMs: MHD instabilities at the transport barrier. *Plasma Physics and Controlled Fusion*, 47(12B):B165, 2005.

[4] P. Maget, J.-F. Artaud, M. Bcoulet, T. Casper, J. Faustin, J. Garcia, G. T. A. Huijsmans, A. Loarte, and G. Saibene. MHD stability of the pedestal in ITER scenarios. *Nuclear Fusion*, 53(9):093011, 2013.

[5] P. B. Snyder, H. R. Wilson, J. R. Ferron, L. L. Lao, A. W. Leonard, T. H. Osborne, A. D. Turnbull,

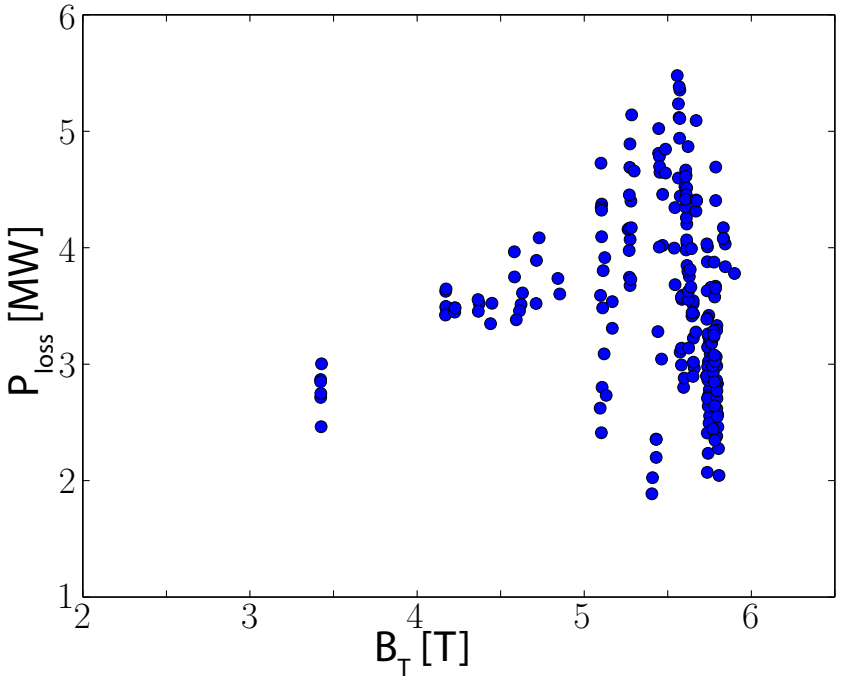

Figure 14: Toroidal field B_T versus loss power P_{loss} in the I-mode dataset. The upper bound of P_{loss} available in I-mode is strictly bound by a linear relation with B_T, indicative of the upper bound of I-mode access (above this power level, the plasma transitions to H-mode). However, below this upper bound the data range in P_{loss} is well-covered.

D. Mossessian, M. Murakami, and X. Q. Xu. Edge localized modes and the pedestal: A model based on coupled peeling–ballooning modes. *Physics of Plasmas*, 9(5):2037–2043, 2002.

[6] H. Zohm. Edge localized modes (ELMs). *Plasma Physics and Controlled Fusion*, 38(2):105, 1996.

[7] M. Keilhacker, G. Becker, K. Bernhardi, A. Eberhagen, M. ElShaer, G. FuBmann, O. Gehre, J. Gernhardt, G. v. Gierke, E. Glock, G. Haas, F. Karger, S. Kissel, O. Kluber, K. Kornherr, K. Lackner, G. Lisitano, G. G. Lister, J. Massig, H. M. Mayer, K. McCormick, D. Meisel, E. Meservey, E. R. Muller, H. Murmann, H. Niedermeyer, W. Poschenrieder, H. Rapp, B. Richter, H. Rohr, F. Ryter, F. Schneider, S. Siller, P. Smeulders, F. Soldner, E. Speth, A. Stabler, K. Steinmetz, K.-H. Steuer, Z. Szymanski, G. Venus, O. Vollmer, and F. Wagner. Confinement studies in L and H-type ASDEX discharges. *Plasma Physics and Controlled Fusion*, 26(1A):49, 1984.

[8] ITER Physics Expert Group on Confinement, Transport and ITER Physics Expert Group on Confinement Modelling and Database, and ITER Physics Basis Editors. Chapter 2: Plasma confinement and transport. *Nuclear Fusion*, 39(12):2175, 1999.

[9] M. Shimada, D. J. Campbell, V. Mukhovatov, M. Fujiwara, N. Kirneva, K. Lackner, M. Nagami, V. D. Pustovitov, N. Uckan, J. Wesley, N. Asakura, A. E. Costley, A. J. H. Donné, E. J. Doyle, A. Fasoli, C. Gormezano, Y. Gribov, O. Gruber, T. C. Hender, W. Houlberg, S. Ide, Y. Kamada, A. Leonard, B. Lipschultz, A. Loarte, K. Miyamoto, V. Mukhovatov, T. H. Osborne, A. Polevoi, and A. C. C. Sips. Chapter 1: Overview and summary. *Nuclear Fusion*, 47(6):S1, 2007.

[10] A. Loarte, G. Saibene, R. Sartori, D. Campbell, M. Becoulet, L. Horton, T. Eich, A. Herrmann, G. Matthews, N. Asakura, A. Chankin, A. Leonard, G. Porter, G. Federici, G. Janeschitz, M. Shimada, and M. Sugihara. Characteristics of type I ELM energy and particle losses in

existing devices and their extrapolation to ITER. *Plasma Physics and Controlled Fusion*, 45(9):1549, 2003.

[11] G. Federici, A. Loarte, and G. Strohmayer. Assessment of erosion of the ITER divertor targets during type I ELMs. *Plasma Physics and Controlled Fusion*, 45(9):1523, 2003.

[12] L. R. Baylor, N. Commaux, T. C. Jernigan, S. J. Meitner, S. K. Combs, R. C. Isler, E. A. Unterberg, N. H. Brooks, T. E. Evans, A. W. Leonard, T. H. Osborne, P. B. Parks, P. B. Snyder, E. J. Strait, M. E. Fenstermacher, C. J. Lasnier, R. A. Moyer, A. Loarte, G. T. A. Huijsmans, and S. Futatani. Reduction of edge localized mode intensity on DIII-D by on-demand triggering with high frequency pellet injection and implications for ITER. *Physics of Plasmas*, 20(8):082513, 2013.

[13] P. T. Lang, A. Burckhart, M. Bernert, L. Casali, R. Fischer, O. Kardaun, G. Kocsis, M. Maraschek, A. Mlynek, B. Plöckl, M. Reich, F. Ryter, J. Schweinzer, B. Sieglin, W. Suttrop, T. Szepesi, G. Tardini, E. Wolfrum, D. Zasche, H. Zohm, and the ASDEX Upgrade Team. ELM pacing and high-density operation using pellet injection in the ASDEX Upgrade all-metal-wall tokamak. *Nuclear Fusion*, 54(8):083009, 2014.

[14] T. E. Evans, R. A. Moyer, P. R. Thomas, J. G. Watkins, T. H. Osborne, J. A. Boedo, E. J. Doyle, M. E. Fenstermacher, K. H. Finken, R. J. Groebner, M. Groth, J. H. Harris, R. J. La Haye, C. J. Lasnier, S. Masuzaki, N. Ohyabu, D. G. Pretty, T. L. Rhodes, H. Reimerdes, D. L. Rudakov, M. J. Schaffer, G. Wang, and L. Zeng. Suppression of large edge-localized modes in high-confinement DIII-D plasmas with a stochastic magnetic boundary. *Physical Review Letters*, 92:235003, Jun 2004.

[15] T. E. Evans, R. A. Moyer, K. H. Burrell, M. E. Fenstermacher, I. Joseph, A. Leonard, T. H. Osborne, G. Porter, M. J. Schaffer, P. B. Snyder, P. R. Thomas, J. G. Watkins, and W. P. West. Edge stability and transport control with resonant magnetic perturbations in collisionless tokamak plasmas. *Nature Physics*, 2:419–423, 2006.

[16] M. Greenwald, R. Boivin, P. Bonoli, R. Budny, C. Fiore, J. Goetz, R. Granetz, A. Hubbard, I. Hutchinson, J. Irby, B. LaBombard, Y. Lin, B. Lipschultz, E. Marmar, A. Mazurenko, D. Mossessian, T. Sunn Pedersen, C. S. Pitcher, M. Porkolab, J. Rice, W. Rowan, J. Snipes, G. Schilling, Y. Takase, J. Terry, S. Wolfe, J. Weaver, B. Welch, and S. Wukitch. Characterization of enhanced D_α high-confinement modes in Alcator C-Mod. *Physics of Plasmas*, 6(5):1943–1949, 1999.

[17] A. E. Hubbard, R. L. Boivin, R. S. Granetz, M. Greenwald, J. W. Hughes, I. H. Hutchinson, J. Irby, B. LaBombard, Y. Lin, E. S. Marmar, A. Mazurenko, D. Mossessian, E. Nelson-Melby, M. Porkolab, J. A. Snipes, J. Terry, S. Wolfe, S. Wukitch, B. A. Carreras, V. Klein, and T. Sunn Pedersen. Pedestal profiles and fluctuations in C-Mod enhanced D-alpha H-modes. *Physics of Plasmas*, 8(5):2033–2040, 2001.

[18] K. H. Burrell, M. E. Austin, D. P. Brennan, J. C. DeBoo, E. J. Doyle, P. Gohil, C. M. Greenfield, R. J. Groebner, L. L. Lao, T. C. Luce, M. A. Makowski, G. R. McKee, R. A. Moyer, T. H. Osborne, M. Porkolab, T. L. Rhodes, J. C. Rost, M. J. Schaffer, B. W. Stallard, E. J. Strait, M. R. Wade, G. Wang, J. G. Watkins, W. P. West, and L. Zeng. Quiescent H-mode plasmas in the DIII-D tokamak. *Plasma Physics and Controlled Fusion*, 44(5A):A253, 2002.

[19] W. Suttrop, V. Hynnen, T. Kurki-Suonio, P. T. Lang, M. Maraschek, R. Neu, A. Stäbler, G. D. Conway, S. Hacquin, M. Kempenaars, P. J. Lomas, M. F. F. Nave, R. A. Pitts, K.-D. Zastrow, the ASDEX Upgrade team, and contributors to the JET-EFDA workprogramme. Studies of the 'quiescent H-mode' regime in ASDEX Upgrade and JET. *Nuclear Fusion*, 45(7):721, 2005.

[20] D. G. Whyte, A. E. Hubbard, J. W. Hughes, B. Lipschultz, J. E. Rice, E. S. Marmar, M. Greenwald, I. Cziegler, A. Dominguez, T. Golfinopoulos, N. Howard, L. Lin, R. M. McDermott, M. Porkolab, M. L. Reinke, J. Terry, N. Tsujii, S. Wolfe, S. Wukitch, Y. Lin, and the Alcator C-Mod Team. I-mode: an H-mode energy confinement regime with L-mode particle transport in Alcator C-Mod. *Nuclear Fusion*, 50(10):105005, 2010.

[21] A. E. Hubbard, D. G. Whyte, R. M. Churchill, I. Cziegler, A. Dominguez, T. Golfinopoulos,

J. W. Hughes, J. E. Rice, I. Bespamyatnov, M. J. Greenwald, N. Howard, B. Lipschultz, E. S. Marmar, M. L. Reinke, W. L. Rowan, J. L. Terry, and the Alcator C-Mod Group. Edge energy transport barrier and turbulence in the I-mode regime on Alcator C-Mod. *Physics of Plasmas*, 18(5):056115, 2011.

[22] J. R. Walk, J. W. Hughes, A. E. Hubbard, J. L. Terry, D. G. Whyte, A. E. White, S. G. Baek, M. L. Reinke, C. Theiler, R. M. Churchill, J. E. Rice, P. B. Snyder, T. Osborne, A Dominguez, and I. Cziegler. Edge-localized mode avoidance and pedestal structure in I-mode plasmas. *Physics of Plasmas*, 21(5):056103, 2014.

[23] John R. Walk. *Pedestal Structure and Stability in High-Performance Plasmas on Alcator C-Mod*. Sc.D. thesis, Massachusetts Instituite of Technology, 2014.

[24] I. H. Hutchinson, R. Boivin, F. Bombarda, P. Bonoli, S. Fairfax, C. Fiore, J. Goetz, S. Golovato, R. Granetz, M. Greenwald, S. Horne, A. Hubbard, J. Irby, B. LaBombard, B. Lipschultz, E. Marmar, G. McCracken, M. Porkolab, J. Rice, J. Snipes, Y. Takase, J. Terry, S. Wolfe, C. Christensen, D. Garnier, M. Graf, T. Hsu, T. Luke, M. May, A. Niemczewski, G. Tinios, J. Schachter, and J. Urbahn. First results from Alcator C-Mod. *Physics of Plasmas*, 1(5):1511–1518, 1994.

[25] N. T. Howard, M. Greenwald, and J. E. Rice. Characterization of impurity confinement on Alcator C-Mod using a multi-pulse laser blow-off system. *Review of Scientific Instruments*, 82(3):033512, 2011.

[26] Arturo Dominguez. *Study of Density Fluctuations and Particle Transport at the Edge of I-Mode Plasmas*. PhD thesis, Massachusetts Institute of Technology, 2012.

[27] J. P. Christiansen, J. G. Cordey, K. Thomsen, A. Tanga, J. C. DeBoo, D. P. Schissel, T. S. Taylor, O. J. W. F. Kardaun, F. Wagner, F. Ryter, S. M. Kaye, Y. Miura, N. Suzuki, M. Mori, T. Matsuda, H. Tamai, T. Takizuka, S.-I. Itoh, and K. Itoh. Global energy confinement H-mode database for ITER. *Nuclear Fusion*, 32(2):291, 1992.

[28] P. N. Yushmanov, T. Takizuka, K. S. Riedel, O. J. W. F. Kardaun, J. G. Cordey, S. M. Kaye, and D. E. Post. Scalings for tokamak energy confinement. *Nuclear Fusion*, 30(10):1999, 1990.

[29] J. W. Hughes, D. A. Mossessian, A. E. Hubbard, B. LaBombard, and E. S. Marmar. Observations and empirical scalings of the high-confinement mode pedestal on Alcator C-Mod. *Physics of Plasmas*, 9(7):3019–3030, 2002.

[30] Y. R. Martin, T. Takizuka, and the ITPA CDBM H-mode Threshold Database Working Group. Power requirement for accessing the H-mode in ITER. *Journal of Physics: Conference Series*, 123(1):012033, 2008.